REVIEW ARTICLE

JSUM ultrasound elastography practice guidelines: basics and terminology

Tsuyoshi Shiina

Abstract Ten years have passed since the first commercial equipment for elastography was released; since then clinical utility has been demonstrated. Nowadays, most manufacturers offer an elastography option. The most widely available commercial elastography methods are based on strain imaging, which uses external tissue compression and generates images of the resulting tissue strain. However, imaging methods differ slightly among manufacturers, which results in different image characteristics, for example, spatial and temporal resolution, and different recommended measurement conditions. In addition, many manufacturers have recently provided a shear wave-based method, providing stiffness images based on shear wave propagation speed. Each method of elastography is designed on the basis of assumptions of measurement conditions and tissue properties. Thus, we need to know the basic principles of elastography methods and the physics of tissue elastic properties to enable appropriate use of each piece of equipment and to obtain more precise diagnostic information from elastography. From this perspective, the basic section of this guideline aims to support practice of ultrasound elastography.

T. Shiina (✉)
Department of Human Health Sciences, Graduate School of Medicine, Kyoto University, Kyoto, Japan
e-mail: shiina.tsuyoshi.6w@kyoto-u.ac.jp

Introduction

Tissue elasticity is an important characteristic which is deeply related with pathological state; For example, in case of breast tumor, most cancerous lesions become harder than normal gland tissue [1–3]. Therefore, elastography has been developed as a modality which provides novel diagnostic information regarding tissue stiffness by replacing the conventional palpation which was used for breast examination. Moreover, recently elastography has found wider applications than breast cancer diagnosis, such as in arteriosclerosis, chronic hepatitis, myocardial diseases, and monitoring for therapy by high-intensity focused ultrasound (HIFU). Ten years have passed since the first practical equipment for elastography was released in 2003 and clinical utility was demonstrated. As a result nowadays each company provides equipment which can offer elastography. The most widely available commercial elastography methods are based on "strain imaging," using external tissue compression and generating images of the resulting tissue strain. In addition, many manufacturers have provided "shear wave imaging," which provides stiffness images based upon the shear wave propagation speed. As a result, the features of each method and equipment, i.e., their merits and limitations, must be clear for their appropriate use.

The Japan Society of Ultrasonics in Medicine (JSUM) ultrasound elastography practice guidelines are written to guide users of ultrasound elastography to comprehend the features of pieces of equipment and fully utilize them for appropriate diagnosis and therapy. Guidelines consist of plural parts; the basic part aims to definitely explain the features of each method and the terminology of the elastography technologies.

Mechanical properties of tissues [4–7]

Static properties and strain

As shown by the use of palpation as a way to diagnose diseases such as breast cancer, the stiffness of tissue reflects the pathological change of tissue. Since stiffness is resistance to deformation, application of external force is required to measure stiffness of tissue. Deformation of tissue is controlled by *elasticity* and *viscosity*. Regarding elasticity, the *stress* σ (equal to the external force per unit area) is proportional to the *strain* ε (equal to the expansion per unit length), as in Hooke's law in Eq. (1), whose coefficient is the *elastic modulus* Γ.

$$\sigma_1 = \Gamma \cdot \varepsilon. \tag{1}$$

Regarding the viscosity component, the stress σ is proportional to the speed of deformation, i.e., the strain rate $d\varepsilon/dt$, through a coefficient μ known as the *viscosity coefficient*.

$$\sigma_2 = \mu \frac{d\varepsilon}{dt}. \tag{2}$$

The mechanical characteristics of general tissue consist of a complex combination of elastic and viscous components, which are often approximated using a simplified model such as the Kelvin–Voigt model.

In cases where the speed of the applied external force is slow, such as manual compression, the effect of viscosity can be disregarded. Conversely, if high-frequency vibration is applied, the viscous component will have a major effect, the extent of which will depend on the frequency.

With regard to elasticity, three types of elastic modulus (Young's modulus, shear modulus, and bulk modulus) are defined based on the method of deformation. The *Young's modulus E* is defined by the following equation when stress is applied longitudinally to a long, thin cylindrical object and strain occurs as shown in Fig. 1a:

$$\sigma = E \cdot \varepsilon_L, \tag{3}$$

where σ is the stress and $\varepsilon_L = \Delta L/L$ is the (longitudinal) strain.

In the absence of volume change, a cylindrical object becomes thinner when stretched as shown in Fig. 1. The percentage change in the radial direction, $\varepsilon_r = \Delta r/r$, is called the transverse strain, and the ratio of longitudinal strain to transverse strain,
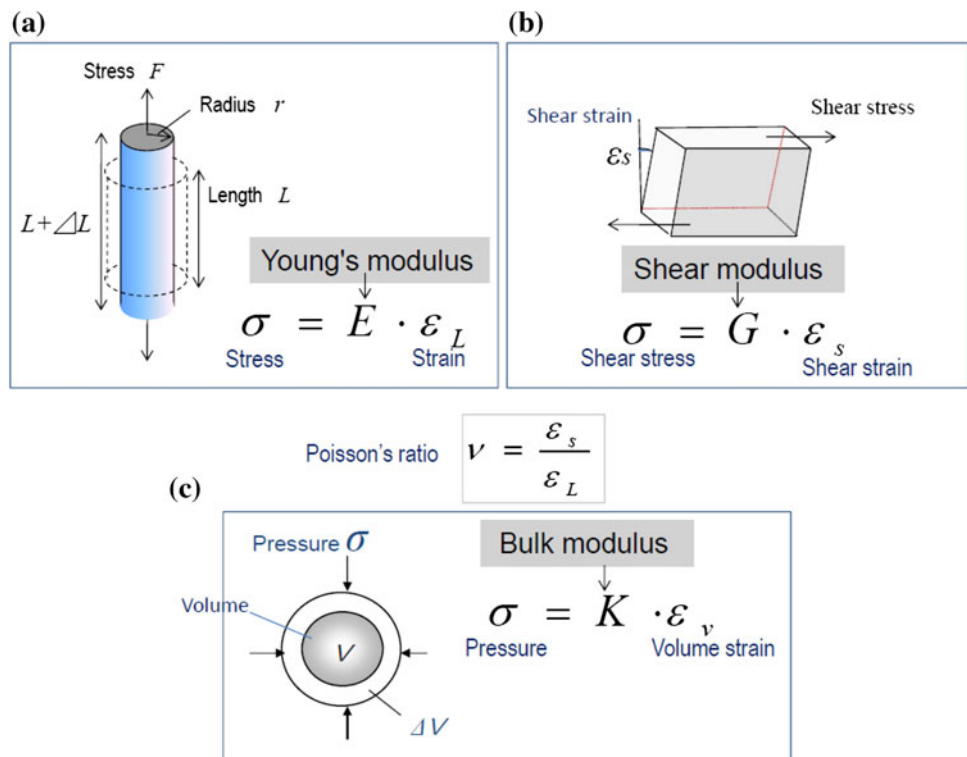
$$v = \frac{\varepsilon_r}{\varepsilon_L}, \tag{4}$$

is called *Poisson's ratio*. Poisson's ratio indicates the extent of volume change caused by deformation, and v will be no higher than 0.5, which applies in the case of an incompressible medium.

The *shear modulus G* is defined by the following equation for the shear deformation, as shown in Fig. 1b:

$$\sigma = G \cdot \varepsilon_s, \tag{5}$$

where $\varepsilon_s = \theta$ is the shear strain.

Fig. 1 Various elastic moduli

The *bulk modulus* K is defined by the following equation when the volume changes under pressure as shown in Fig. 1c:

$$\sigma = K \cdot \varepsilon_v, \tag{6}$$

where $\varepsilon_v = \Delta V / V$ is the volume strain. The larger the elastic modulus is, the smaller the strain will be for the same stress, so the material will be stiffer. These three elastic moduli are related to each other; For example, the Young's modulus E can be expressed as in Eq. (7) using the shear modulus G and Poisson's ratio v. The water content of soft tissue is high, and consequently its Poisson's ratio is near the value of 0.5 for an incompressible medium, so the Young's modulus will be equal to about three times the shear modulus, as in the following equation:

$$\begin{aligned} E &= 2(v+1)G \\ &\approx 3G. \end{aligned} \tag{7}$$

Dynamic properties and shear wave speed

The elastic modulus also determines the propagation speed of waves. Wave propagation generally involves *longitudinal waves* and *transverse waves*. The speed c_L of the longitudinal waves which are used for ordinary pulse echo images is expressed as

$$c_L = \sqrt{\frac{K}{\rho}}, \tag{8}$$

where ρ indicates the density of the medium. Using the shear modulus, the speed c_s of transverse waves is expressed as

$$c_s = \sqrt{\frac{G}{\rho}}. \tag{9}$$

In the case of soft tissue, it is known that the speed of a longitudinal wave is about the same as the speed of sound in water ($c_L = 1500$ m/s), but this means that there is little difference in K between tissues. In contrast, transverse waves, which are also called *shear waves*, attenuate rapidly and disappear in the MHz ultrasound band, but attenuation decreases and they can propagate in vivo when the frequency is below about 1 kHz. Moreover, their velocity is quite slow, i.e., $c_s = 1$–10 m/s, as compared with longitudinal waves, so G is low, i.e., 1–100 kPa, and the difference between tissues is large, enabling reconstruction of images with high tissue contrast [5].

On the other hand, unlike static deformation, *velocity dispersion* caused by the viscosity occurs during wave propagation when the frequency is high in soft tissues; For example, when the Kelvin–Voigt model is used, the following equation is used for the speed of a transverse wave

instead of Eq. (9) as a result of taking into account viscosity [8]:

$$c_s = \sqrt{\frac{2\left\{ G^2 + (2\pi\mu f)^2 \right\}}{\rho \left\{ G + \sqrt{G^2 + (2\pi\mu f)^2} \right\}}}. \tag{10}$$

Thus, c_s becomes a function of frequency f, and the higher the frequency is, the faster the speed will be.

Principle of elastography

Measured physical quantity

As mentioned in the previous section, differences in the elasticity of soft tissue are expressed by elastic moduli such as the Young's modulus E or shear modulus G.

The elastic modulus can be estimated in the following two ways according to directly measured quantities:

Strain imaging

In this method, one measures the strain ε on externally applying a stress σ, calculating E using the following equation:

$$E = \sigma / \varepsilon. \tag{11}$$

However, in practice, instead of elastic modulus, strain is used by assuming that stress is uniform, since it is difficult to know the stress within the body.

Shear wave imaging

In this method, one measures the propagation speed c_s of shear waves, calculating E or G by using Eq. (12).

$$E \approx 3G = 3\rho c_s^2. \tag{12}$$

Here, we assume that the Poisson's ratio of soft tissue is near the value of 0.5 for an incompressible medium, and that other conditions such as constant density, homogeneity, and isotropy are satisfied. Thus, the Young's modulus will be equal to about three times the shear modulus.

Excitation methods

Both of the above methods require external excitation (compression or vibration) to produce a reaction such as deformation or shear wave propagation, and a physical quantity such as strain or propagation speed is measured by using ultrasound to estimate the elasticity.

Excitation methods can be classified into (a) manual compression (using hand or cardiovascular pulsation), (b) acoustic radiation force impulse, and (c) mechanical impulse.

Classification of elastography methods

As explained in the previous section, there are two major methods based on different types of measured physical quantities and three ways to apply external excitation. Therefore, elastography is classified as presented in Table 1. Methods for integration into clinical practice are categorized into four groups as follows:

1. Stain elastography

Strain induced by quasistatic methods such as manual compression or cardiovascular pulsation is measured, and the distribution of strain or displacement within a region of interest (ROI) is displayed.

2. Acoustic radiation force impulse (ARFI) imaging

A focused acoustic radiation force "push" pulse is used to deform the tissue. The resulting tissue displacement is monitored. Although strain is the spatial differential of displacement, they are similar since both are inversely related to the tissue stiffness.

3. Shear wave elastography

Acoustic radiation force is used to generate shear waves within the organ of interest. The distribution of speed or elastic modulus converted by Eq. (12) is displayed. There is also a method which measures a local average of shear wave speed, not for imaging.

4. Transient elastography

A mechanical impulse or vibrating "punch" is used to generate shear waves. At present, commercialized technology is specialized for measuring stiffness of liver tissues and not for imaging.

The outputs obtained by each elastography technology correspond to a measured physical quantity. For strain, this includes geometric measures such as the size or shape of a low-strain area, the strain ratio of the lesion to a reference, and the E/B size ratio (the ratio of the size of a lesion in a strain image to its size in a B-mode image). For shear wave-based methods, the physical quantity is the speed itself and/or the Young's modulus converted from the shear wave speed by using Eq. (12).

Practical elastography systems

Strain elastography

The basic idea of strain elastography, i.e., measuring the tissue deformation generated by manually applying pressure with a probe on the body surface, similar to an ordinary ultrasound examination was proposed by Dr. Ophir about 20 years ago [9, 10].

Table 1 Classification of various elastography methods

Elastography methods
a)Measured physical quantity
b)Output
 	
Excitation methods
	Strain imaging
	a)Strain (displacement)
	b)Geometric measures
	  ·Strain ratio
	  ·E/B size ratio
			Shear wave imaging
			a)Shear wave speed
			b)Shear wave speed, Young's modulus	

(A)Manual compression -Palpation, -Cardiovascular pulsation	**Strain elastography** -Real-time tissue elastography™ -Elastography -ElastoScan™ -eSieTouch™Elasticity Imaging	(Hitachi Aloka) (GE, Philips, Toshiba) (Samsung) (Siemens)		
(B)Acoustic radiation force impulse	**ARFI Imaging** -Virtual Touch™Imaging	(Siemens)	**Shear wave elastography** -ShearWave™ Elastography: SWE -Virtual Touch™ IQ: VTIQ -Virtual Touch™ Quantification: VTQ -ElastPQ™	(SSI) (Siemens) (Siemens) (Philips))
(C)Mechanical vibration and impulse			**Transient elastography** -FibroScan™	(EchoSens)

As shown in Fig. 2, when very slight pressure (strain is about 1 %) is applied to tissue with a probe in the beam direction, the majority of the displacement will be in the direction of propagation of the ultrasound pulse, and the tissue deformation can be approximated using a one-dimensional (1D) spring model. The displacement $\delta(z)$ at each site z in the beam direction of the tissue is then calculated. This is obtained by calculating the correlation between the echo signal before and after compression. Next, the strain ε is obtained as the spatial differential of the displacement, that is, the ratio of the difference in displacement between two points to their distance pre-compression, L, as shown in Eq. (13).

$$\varepsilon = \frac{\delta_2 - \delta_1}{L}. \tag{13}$$

In fact, as described below, many technologies had to be developed to achieve real-time capability, accuracy, and stability during manual compression before it became available for clinical application [11–15].

As shown in Eq. (11), the Young's modulus E can be obtained if the stress σ and strain ε are known. However, since it is difficult to calculate the stress distribution in vivo, it is assumed to be uniform. As a result, stiff segments with large elastic modulus E will have small strain ε; therefore, strain serves as a useful indicator from the standpoint of evaluating relative stiffness.

The first practical system for ultrasound elastography was based on *strain elastography* and released in 2003 (Fig. 3). Its efficacy was demonstrated in the diagnosis of breast cancer tumors together with the elasticity score, which was proposed at the same time [16, 17] and is currently being used in various fields of clinical medicine. Nowadays, many manufacturers produce ultrasonographic equipment with a strain imaging function, as presented in Table 1.

Display methods for strain images

Strain elastography has the advantages of being easy to use and providing elasticity images with high spatial resolution in a manner similar to palpation, i.e., tissue deformation. On the other hand, strain is a relative indicator of stiffness that changes depending on the degree of compression. So, for example, the elastogram shown in Fig. 3b displays the strain normalized by the mean within the ROI in order to obtain stable images without being subject to fluctuations in the intensity of compression.

In addition, the display method of elastograms is important to relate the location in the elastogram to B-mode images. Different types of display method are used for ultrasonographic equipment, as shown in Fig. 4; For example, Dr. Ueno proposed the method applied in the first practical equipment [17]: a translucent elastogram (showing normalized strain) is superimposed in color on the corresponding B-mode image; the mean strain in the ROI is indicated in green, areas of low strain as stiff tissue in blue, and areas of high strain as soft tissue in red, as shown in Fig. 4a. Another type of display method is to display the elastogram in gray scale and the B-mode image side by side, as shown in Fig. 4b. In this case, the location in the elastogram can be indicated on the B-mode image by a cursor.

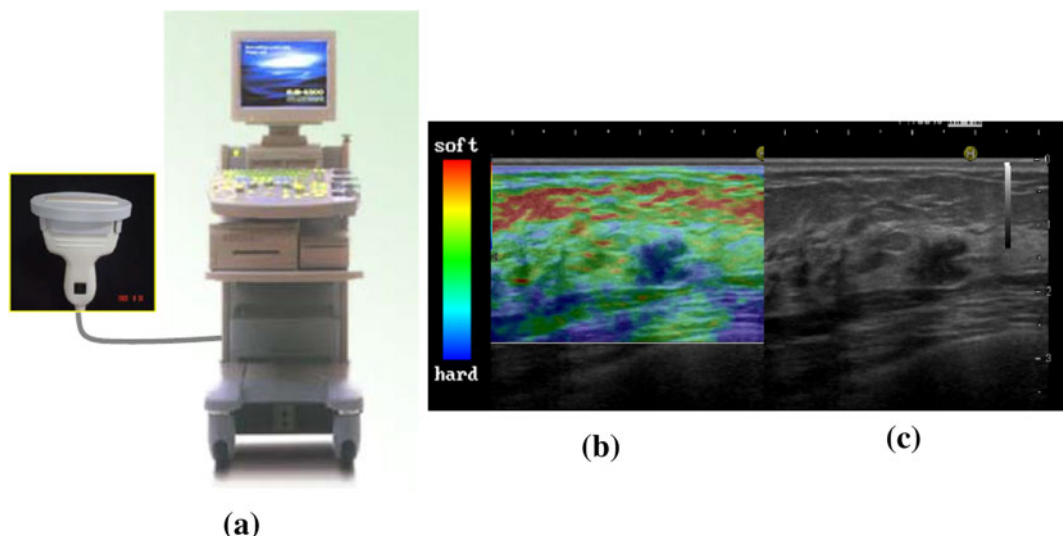**Fig. 2** Principle of strain elastography
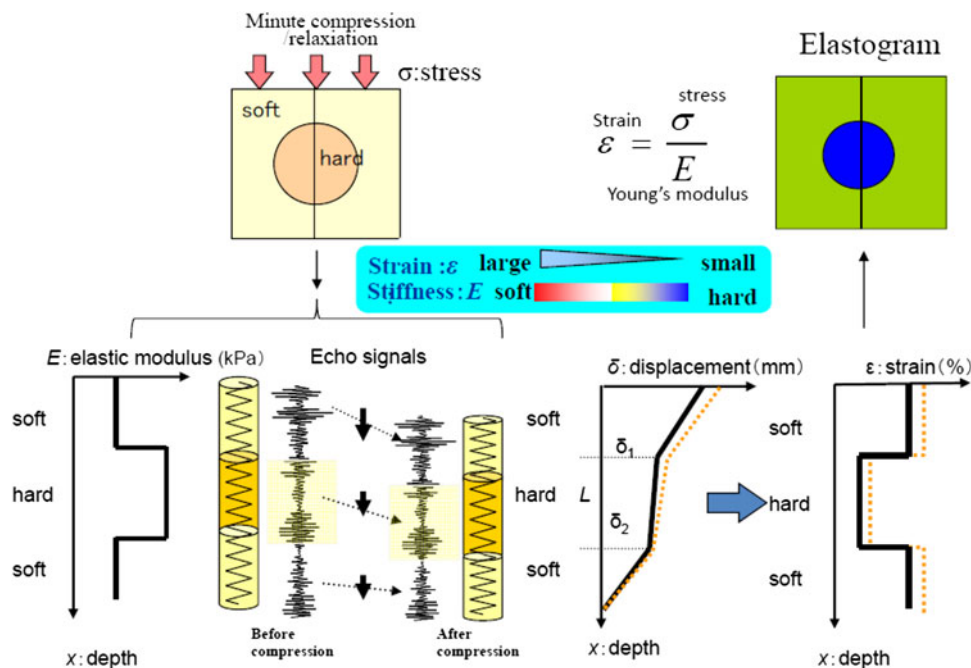
Fig. 3 Practical application of strain elastography. **a** First practical ultrasound elastography equipment, which was released for breast examination in 2003 (Real-Time Tissue Elastography, Hitachi Aloka Ltd.). **b** Elastogram (breast cancer). **c** B-mode

Fig. 4 Different display methods for strain images. **a** Display method applied in the first practical elastography system: the translucent elastogram within the ROI is superimposed in color on the corresponding B-mode image; the average strain in the ROI is indicated in green, areas of low strain as stiff tissue in blue, and areas of high strain as soft tissue in red (courtesy of Hitachi Aloka Medical). **b** Other display methods: elastogram superimposed on B-mode image with different color (center) and elastogram in gray scale (right) (courtesy of Siemens)


ε_0: Mean strain within ROI

(a)

(b)
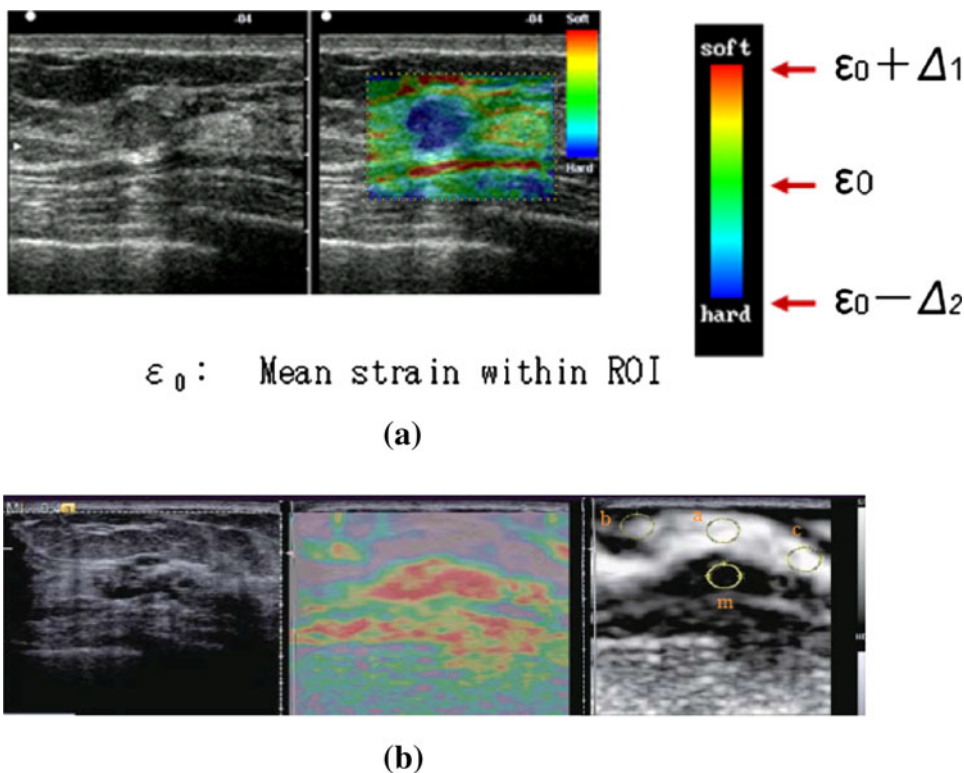
Elasticity score

Strain images depict the relative difference in elasticity between a lesion such as a mass and the surrounding tissue. Therefore, this method is suitable for detecting patterns in images. In fact, the elasticity score (Tsukuba score) is being used for breast cancer diagnosis [17]. The elasticity score is a five-point scale used to classify elastography patterns from benign to malignant as follows: score 1 (benign), score 2 (benignancy suspected), score 3 (difficult to distinguish between benign/malignant), score 4 (malignancy suspected), and score 5 (malignancy strongly suggested), as shown in Fig. 5. In the case of cysts, a specific blue–green–red pattern called the BGR sign is seen from the body surface side. This is a type of artifact, which is caused by the low level of the internal echo signals from a

Fig. 5 Elasticity score in breast cancer diagnosis
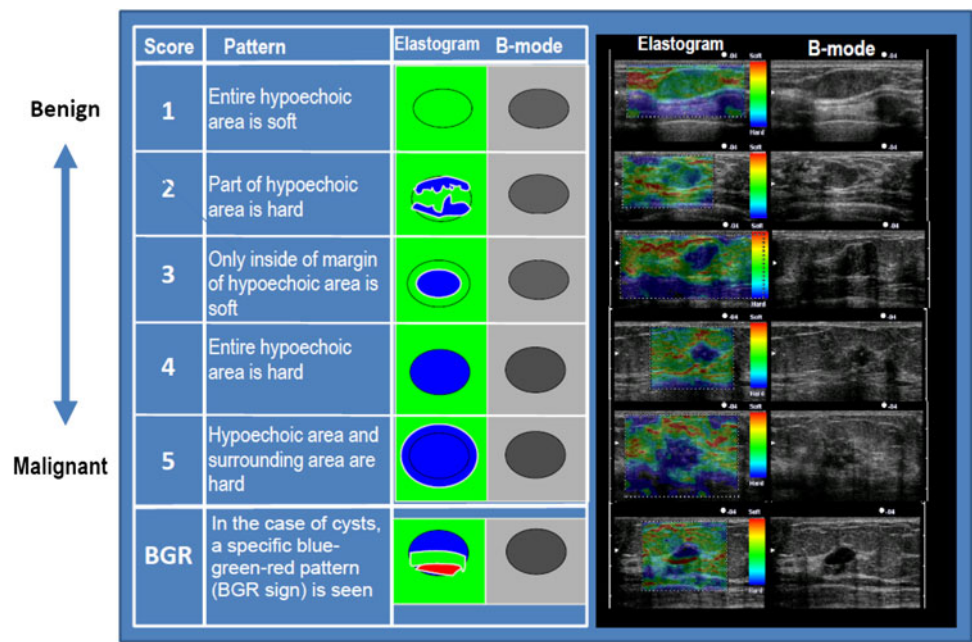
cyst but this can be used for cyst diagnosis, like a lateral shadow on B-mode images.

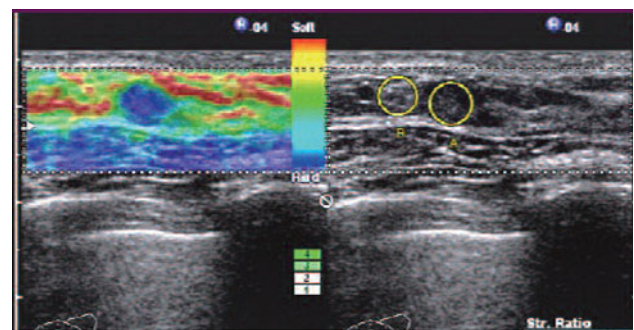*Quantitative evaluation based on strain imaging*

Strain imaging is basically qualitative, so it is difficult to perform quantitative comparisons between cases using strain. The fat lesion ratio (FLR) was proposed as a pseudoquantitative method. The FLR is the strain ratio between the fat and the lesion (fat in the mammary gland is used as a reference region where the change in elasticity caused by disease is minimal), as shown in Fig. 6a [18, 19].

The size of the tumor in an elastogram is often measured and compared with the size of the low-echo area in B-mode as shown in Fig. 6b, because it has been reported that malignant tumors often appear larger in strain images than in B-mode images.

Another example is a method for estimating the elastic modulus of a lesion based on the strain ratio using a coupler with known elastic modulus [20]. In addition, from elastograms of diffuse diseases such as chronic hepatitis, morphological and statistical features are extracted and analyzed for evaluation of fibrous stage, as described in the clinical section of this report.

Displacement measurement methods

In strain imaging, displacement in the direction of pulse propagation is measured to calculate strain, while in shear wave imaging, the displacement of tissue in the direction perpendicular to the shear wave propagation is measured to calculate the speed of shear wave propagation. Therefore,
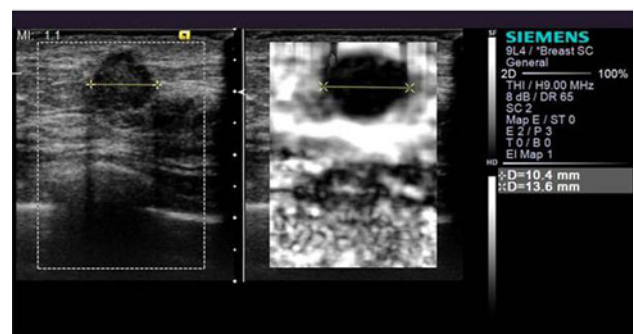
Fig. 6 Quantitative diagnosis based on strain imaging. **a** Measurement of strain ratio (courtesy of Hitachi Aloka). **b** Measurement of tumor size based on elastogram and comparison with B-mode image (courtesy of Siemens)

measurement of displacement is a key technology in all elastography techniques, and there are several methods for measuring it. As presented in Table 1, strain elastography is now installed in ultrasound equipment from many

manufacturers, but each manufacturer uses its own method for measuring displacement, which results in differences in image characteristics such as spatial and temporal resolution and differences in optimal measurement conditions.

The typical methods for measuring displacement are presented below:

Spatial correlation method (speckle tracking method, pattern matching method)

This is a method that tracks the movement of image patterns. The simplest method is to measure the 1D displacement along the beam axis, as shown in Fig. 7a. Echo signals $s(t)$ and $s'(t)$ before and after compression are clipped out in a time window $w(z; t)$, and their cross-correlation coefficient in Eq. (14) is calculated to evaluate the degree of similarity. Calculation of the cross-correlation coefficient is repeated while moving the window, and the displacement is defined as the amount of movement when the value is at its maximum.

$$R(\delta) = \frac{\int x(z;t)y(z+\delta;t)dt}{\sqrt{\int x^2(z;t)dt \int y^2(z+\delta;t)dt}}, \qquad (14)$$

where $x(z; t)$ and $y(z; t)$ are the echo signals clipped out in time window $w(z; t)$ before and after compression, respectively.

In practice, each ROI moves in the azimuthal direction in the cross-section. Therefore, to obtain the displacement more accurately, adjustment is made by performing a two-dimensional (2D) search in both the range direction and the azimuthal direction, as shown in Fig. 7b. In addition, tissue also moves in the slice direction, but the beam width in the slice direction is generally large in the case of an ordinary electronic scanning probe, so the impact is smaller than for the azimuthal direction as long as the cross-section does not deviate much.

Phase difference detection method (Doppler method)

In this method, the phase difference between echo signals obtained by transmitting repeated pulses is detected by an autocorrelation method to calculate the displacement, which is basically the same method as that used in color Doppler and tissue Doppler [21].

The advantages of the Doppler method are its excellent real-time capability and its relative robustness against noise, but only 1D displacement in the beam direction can be measured due to angle dependence, and errors occur due to aliasing when measuring large displacements that exceed half the wavelength.

The advantages of the speckle tracking method are that it is possible to measure even large displacements that exceed the wavelength if the change in the speckle pattern is within a small range and that it is possible to track the movement of the ROI in 2D and three dimensions (3D), as stated above. However, the disadvantage is that the real-time capability may be lost because calculation of correlation requires enormous computational effort. In addition, it is susceptible to the effects of noise, and it is prone to detection errors when the speckle pattern is unclear due to a low echo level, etc.

Combined method

A combined autocorrelation method that combines the merits of the phase difference detection method and the spatial correlation method has been developed [13, 16]. In a clinical case, a wide dynamic range of strain is required, since fluctuations in the speed of compression are large in the case of manual compression. Therefore, a rough displacement is first calculated from the envelope at resolution of half a wavelength, then the displacement is calculated at high resolution using the phase difference by

Fig. 7 Calculation of correlation using the spatial correlation method. **a** Correlation in 1D window. **b** Correlation in 2D window
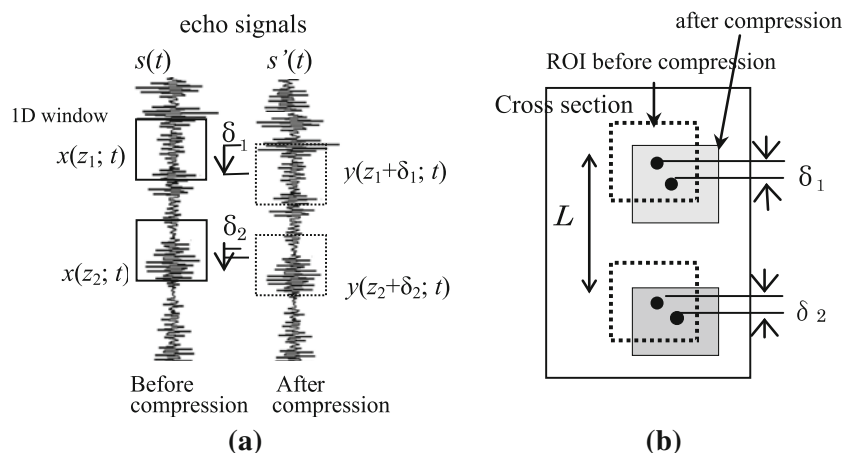
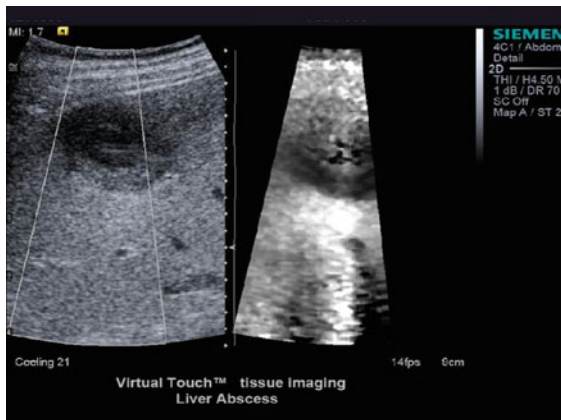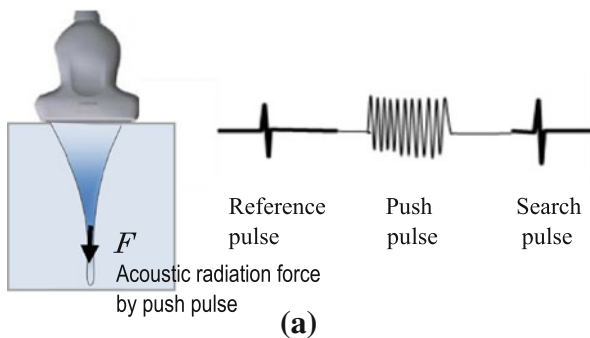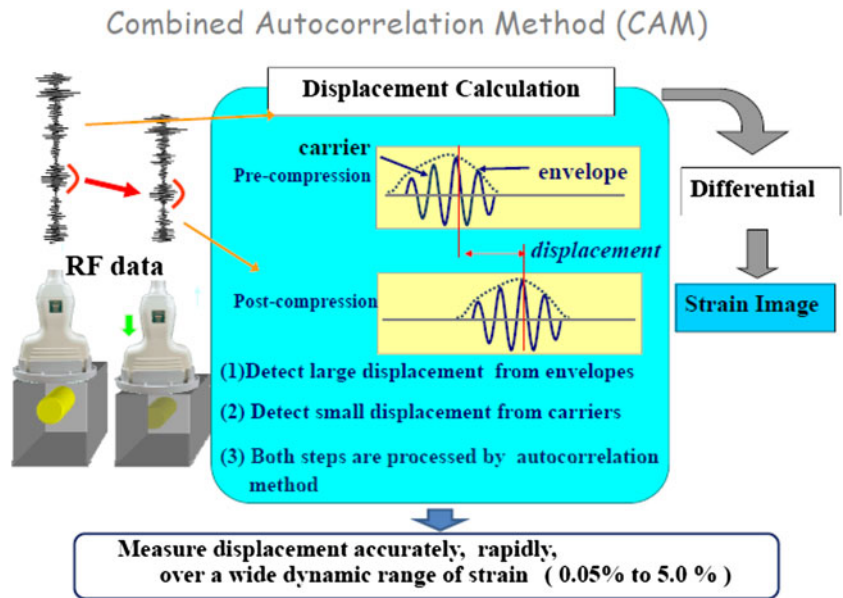**Fig. 8** Principle of the combined autocorrelation method

Fig. 9 Pulse sequence in ARFI imaging and clinical example. **a** Acoustical radiation force by push pulse and pulse sequence in ARFI imaging. ARFI imaging utilizes acoustic push pulses and imaging pulses before and after application of the "push" pulse to monitor the tissue deformation (displacement) within the region of the "push." **b** Clinical example (liver abscess)

correcting the rough displacement as shown in Fig. 8. As a result, this method has a wide dynamic range and provides high accuracy, being able to accommodate strain ranging from about 0.05 to 5 % without causing aliasing errors, for not only displacements of less than a wavelength but also large displacements. Since both processes use the autocorrelation method applied in color Doppler, it achieves high speed, high accuracy, and a wide dynamic range for detecting displacement; as a result, the method is suitable for manual compression. Therefore, it was installed in the first equipment that was put to practical use.

In the case of actual equipment, improvements have been made to the above-mentioned spatial correlation method and phase difference detection method, and they are being used in practical equipment, but differences in their characteristics manifest as differences in frame rate, image quality, measurement conditions, etc.

Acoustic radiation force impulse (ARFI) imaging

While strain elastography relies on manual application of pressure, a strain imaging method that deforms tissue using focused acoustic radiation force has also been devised. This method, called acoustic radiation force impulse (ARFI) imaging [22, 23], became commercially available within the past few years.

In this method, a focused acoustic radiation force "push" pulse is generated according to Eq. (15) [24, 25].

$$F = \frac{2\alpha I}{c}, \tag{15}$$

where α is the absorption coefficient, I is the temporal average intensity of ultrasound, and c is the speed of sound.

Imaging pulses before and after application of the "push" pulse are used to monitor the tissue deformation (displacement) within the region of the "push." The same transducer is used both to generate the push pulse and to monitor the resulting tissue displacement, as shown in Fig. 9a. By sequentially scanning different tissue regions with the focused radiation force, images of tissue displacement that portray relative differences in tissue stiffness are generated (Fig. 9b). The tissue displacement response is directly related to the magnitude of the applied force, and inversely related to the tissue stiffness. These images do not provide quantitative information about tissue stiffness because the magnitude of the applied radiation force varies with tissue attenuation from patient to patient and is difficult to quantify. This imaging approach is implemented commercially as the Siemens Virtual Touch™ feature [26–29].

Appropriate measurement conditions and artifacts in strain imaging

Many manufacturers provide elastography equipment offering strain imaging. In terms of artifacts in strain imaging, it should be noted that commonly the stress distribution is not uniform within the body and the tissue elasticity is nonlinear.

As expressed by Eq. (11), strain is used as an index of stiffness instead of the Young's modulus, under the assumption that the stress is uniform. However, in practice, stress tends to concentrate on curved boundaries, making such areas appear softer than adjacent areas, as shown in Fig. 10. In many cases, this kind of artifact is easily recognized based on a priori information such as tumor shape.

Regarding tissue nonlinearity, in the case of biological tissue, the Young's modulus tends to increase when the compression is intensified, as shown in Fig. 11, and the extent of the increase differs from tissue to tissue [30].
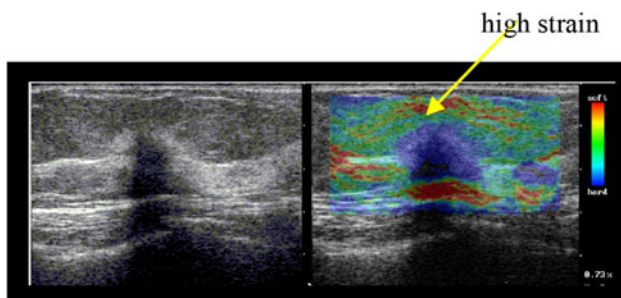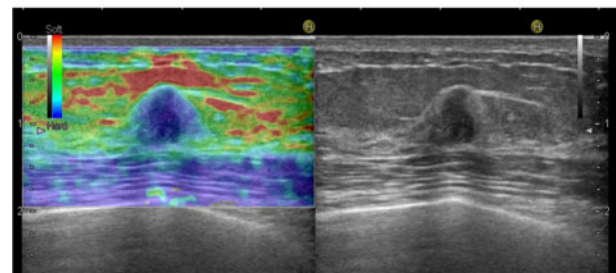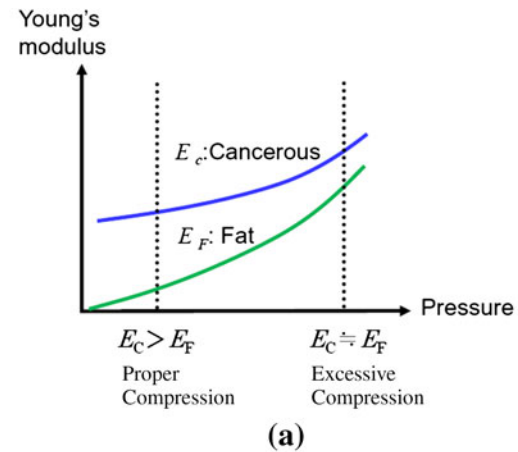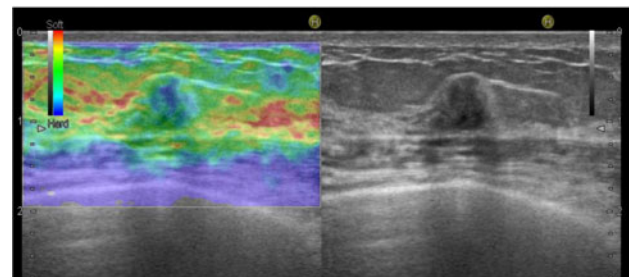

Fig. 10 Artifacts due to stress concentration: breast cancer (scirrhous)

Fig. 11 Effect of excessive compression (breast cancer). **a** Change in contrast according to nonlinearity of tissue elasticity. When compression is increased, the tissue stiffens and the contrast between fat and a cancerous mass decrease. **b** Adequate compression. **c** Excessive compression

For example, when the degree of compression is slight, the difference in the Young's modulus between mammary gland tissue and tumor tissue is large and consequently the tumor tissue is clearly displayed as a relatively low-strain region, as shown in Fig. 11b. However, when the compression is too strong, the stiffness of the mammary gland will increase, and the difference from the tumor tissue will be smaller, possibly resulting in a false-negative finding, as in Fig. 11c.

Such nonlinearity becomes marked when the compression generates strain in excess of several percent. However, when strain of about 1 % is generated in the mammary gland, stability and reproducibility can be achieved even if

the level of compression fluctuates, since it is within the linear range.

Unlike strain elastography based on manual compression, the ARFI imaging approach does not rely on the transducer compression technique, and it has the advantage of being able to focus the "push" within deep-lying organs, where it can be difficult to generate deformation by compression from the body surface. On the other hand, this method can be depth limited, with most commercial implementations reaching a maximum depth of only about 75 % of corresponding B-mode images from a given transducer.

In addition, in order to generate detectable levels of strain, the "push" pulses are of longer duration than regular diagnostic pulses. Therefore, in order to maintain acoustic output within diagnostic limits, current equipment enforces a certain amount of "cooling" time after each measurement, which reduces the frame rate achievable by this imaging technique. Moreover, it is recommended that it not be used in combination with an environment in which a physiological response to sound could easily occur in the body, such as with use of contrast agents [31, 32].

The method that employs acoustic radiation force requires appropriate focusing of pulse waves to apply pressure in order to generate tissue displacement. As such, it can be affected by the inhomogeneous properties of tissue and incident angle of the pushing pulse. In addition, tissue stiffens when the compression applied by the probe is intensified, because of the nonlinearity of tissue elasticity. Therefore, the method employing acoustic radiation force also requires a technique to maintain the optimal conditions.

Shear wave imaging

Shear wave imaging is based on the theory that the speed of shear wave propagation, c_s, through tissues is related to their stiffness [33]. The relation is expressed by Eq. (12); that is, the elastic modulus, E, is proportional to the square of the speed of shear wave propagation, $E = 3\rho c_s^2$, on the assumption of simple, i.e., linear, isotropic, incompressible, and homogeneous, material.

Shear waves can be generated by a variety of sources, including external vibration, physiological motion, and acoustic radiation force.

Transient elastography

In this method, short pulsed and low-frequency (about 50 Hz) vibrations such as those shown in Fig. 12a are applied at the body surface using vibration excitation [34]. The summed contributions of the transversely polarized shear waves coming from subsources on the body surface give rise to a globally longitudinally polarized shear wave on the axis of the vibrator within the body. The displacements induced in the medium by
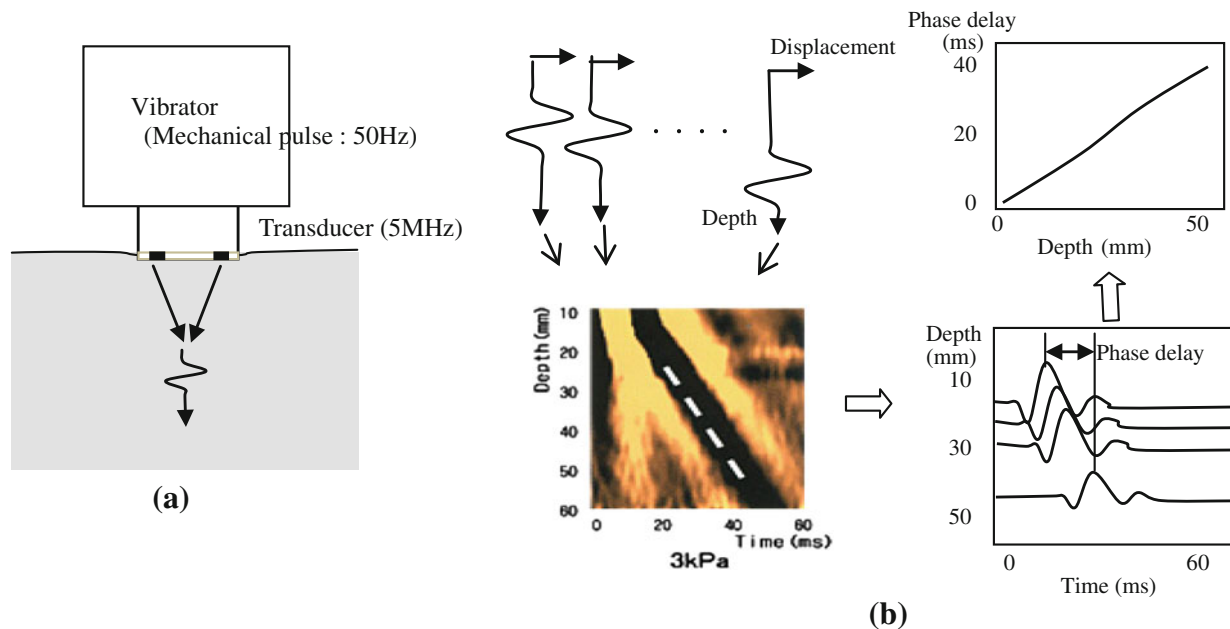

Fig. 12 Principle of transient elastography. a Generation of shear waves by mechanical pulse waves. The summed contributions of the transversely polarized shear waves coming from subsources give rise to a globally longitudinally polarized shear wave on the axis of the vibrator. b M-mode image of displacement estimates and estimation of shear wave speed

Fig. 13 Measurement of propagation speed of shear waves
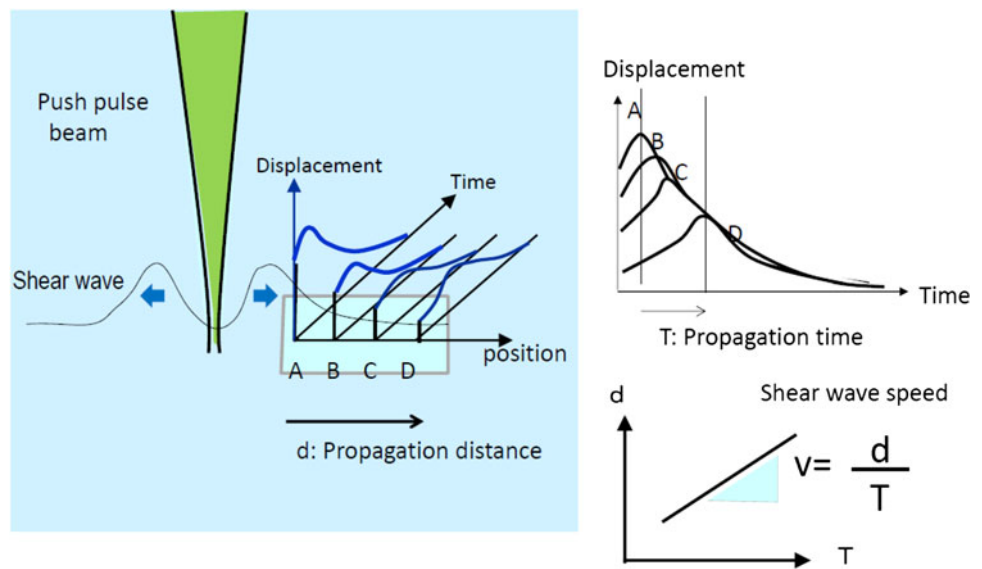
this wave are measured by using an approach similar to the Doppler method. M-mode images are composed of many radio frequency (RF) lines stored while the shear wave propagates inside the medium, as shown in Fig. 12b. The phase delay of the shear wave (shear wave propagation time) is obtained from the peak point of this displacement, and the shear wave propagation speed c_s (m/s) is obtained based on the slope of the relation between phase delay and depth. Using ρ (kg/m^3) as the density, the elasticity (Young's modulus) E (kPa) is calculated as $E = 3\rho c_s^2$. This method is currently used in FibroScan^{TM} for evaluation of liver fibrosis.

Shear wave elastography

In response to focused acoustic radiation force excitation, in addition to vibrating at the ultrasonic frequency, the tissue within the region of excitation (ROE) is also deformed, and shear waves are created and propagate away from the ROE in a direction orthogonal to the excitation beam, as shown in Fig. 13.

The right of Fig. 13 shows the displacement through time profiles at the focal depth of radiation force excitation at four different lateral positions. By comparing this waveform between adjacent positions, the propagation time T is obtained. Shear wave speed estimates are generated by calculating the ratio of distance, d, to propagation time, T. In fact, for improved accuracy, the speed is obtained based on the slope of an approximation line on a graph of distance versus propagation time for a measurement point obtained using multiple detection beams within a sample volume.

Since the acoustic radiation force is applied at a single focal location, imaging requires generation of shear waves at multiple points throughout the imaging area, which

reduces the frame rate. Another approach is to use a multifocal zone configuration in which each focal zone is interrogated in rapid succession, leading to a cylindrically shaped shear wave extending over a greater depth, enabling real-time shear wave images to be formed as shown in Fig. 14. This approach has been termed supersonic shear imaging, as implemented by ShearWave^{TM} elastography (SWE) [35].

Whichever generation method is used, shear wave imaging can be used to calculate the distribution of c_s. Making use of its quantitative capability, it is used not only for imaging but also for numerically calculating tissue elasticity. Although it is a merit of shear wave imaging that the elastic modulus is obtained without estimating stress, it is to be noted that Eq. (12) relies on the assumption of a simple, i.e., linear, isotropic, incompressible, and homogeneous, material.

At the same time, the apparent elasticity associated with the propagation speed will change with internal pressure caused by blood pressure, etc., which may be different from the elasticity caused by fibrosis. In fact, it has been reported that the velocity increases during inflammation due to jaundice [36]. In addition, the apparent elastic modulus $G = \rho c_s^2$ calculated by Eq. (10) will be larger than the elastic modulus obtained by static compression when the viscosity is high. Figure 15 shows the difference in the frequency dependence of velocity due to the presence of viscosity.

Appropriate measurement conditions and artifacts in shear wave imaging

In shear wave imaging, the Young's modulus is estimated by generating shear waves in the body and measuring their propagation speed. Therefore, the measurement conditions

Fig. 14 Shear wave excitation and high-speed measurement by SWE. a Formation of the shear wave wavefront by movement of the push pulse focal point, leading to a cylindrically shaped shear wave extending over a greater depth. b High-speed measurement of displacement by transmitting plane waves and simultaneously performing aperture synthesis with about 5,000 frames/s, an almost 100-fold increase
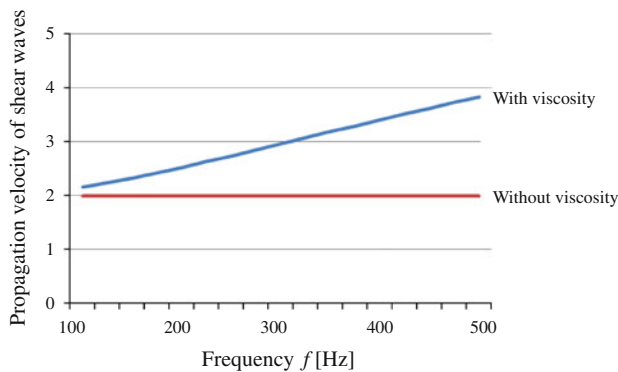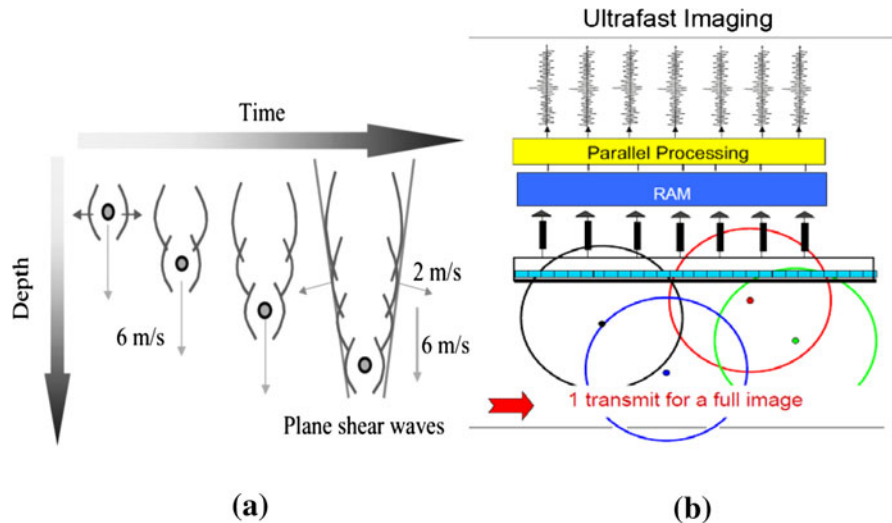

Fig. 15 Difference in propagation velocity according to presence or absence of viscosity ($G = 4$ kPa, $\mu = 3$ Pa s)

to be considered for appropriate imaging and possible artifacts in a clinical setting are as follows:

Insufficient intensity of acoustic radiation force

The method of generating shear waves by tissue compression using an acoustic radiation force requires that pulse waves for excitation appropriately form a focal point in the body. Therefore, when contact between the probe and the surface of the body is inadequate, or when the heterogeneity of acoustic properties of tissue is large, sufficient acoustic force for excitation cannot be achieved at the affected area, resulting in shear waves not being appropriately generated. This causes artifacts and failed measurements.

Effects of refraction/reflection of shear waves

As described in the "Dynamic properties and shear wave speed" section, the range of the distribution of shear waves in tissue is large, i.e., 1–10 m/s, unlike longitudinal waves used in B-mode ultrasound, which travel at approximately the acoustic velocity in water, i.e., about 1,500 m/s. This means that shear waves are strongly refracted at tissue interfaces where the acoustic speed differs. Likewise, the difference in the acoustic impedance of tissue to shear waves is also large, sometimes resulting in the reflection coefficient at a tissue margin being large compared with that for longitudinal waves.

In the case of malignant tumors in particular, the acoustic velocity changes at the tumor site because it is stiffer relative to the surrounding tissue, and the inside of the mass often has a heterogeneous structure and properties; therefore, the wave phenomena caused by refraction and reflection are liable to become marked.

The change in propagation direction caused by refraction must be determined in order to accurately calculate the acoustic velocity of shear waves to obtain the Young's modulus using shear wave imaging. For actual diagnostic equipment, simpler approaches, such as assuming the propagation direction, are applied to emphasize their real-time capability, which is the advantage of ultrasonography. Therefore, although shear wave imaging yields elastic characteristics as numerical values, at the present time, they need to be interpreted carefully, with the understanding that artifacts and variations in measurements will occur.

Relationship between strain and shear wave speed images

Both strain and shear wave speed images provide information related to underlying tissue stiffness. As such, in the absence of artifacts, the correlation between these image types in a given patient is expected to be high. However, when the simplifying assumptions used to derive the

images for the different methods do not accurately reflect the tissue properties, the information provided by each image will be different. One of the important factors is the different frequency range. Strain elastography based on manual compression basically provides static biomechanical properties of tissue, while shear wave imaging represents dynamic properties at a higher frequency range. As a result, there is a possibility that the values of the apparent elastic modulus obtained based on their simple assumptions are different.

Tissue nonlinearity is associated with decreased strain contrast (Fig. 11) and increased shear wave speeds when excessive transducer compression is applied. As a result, for both strain and shear wave imaging, minimizing the amount of transducer compression used during imaging (i.e., to <1 %) will result in the most reproducible imaging scenario. Tissue heterogeneities will also impact both approaches, leading to artifacts arising from reflected waves in shear wave speed images, and strain concentrations surrounding tissue heterogeneities. More detailed investigation of the impact of these assumptions and associated image artifacts should be carried out in the future.

Conclusions

The first practical equipment for elastography was released in 2003, and today every manufacturer offers strain elastography, with many offering both strain and shear wave-based approaches. In addition to breast examination, elastography is now evolving into diagnosis in wider clinical fields including in breast, liver, thyroid, prostate, etc.

On the other hand, it should be noted that there remains an unexplained feature which is required to build the clinical value of elastography and develop more useful equipment, namely disease models that link genetic, cellular, biochemical, and gross pathological changes with observations of biomechanical properties; For example, it is less well understood how biomechanical properties change and are reflected in elasticity images as cancer develops. Development of elastography technology and elucidation of the relation between elasticity images and tissue diseases are connected to each other, since reliable data are provided by high-performance equipment.

At present, as described herein, there are different methods of elastography, each of which has both advantages and weak points. At the same time, this is still an evolving technology and the near future will bring an expanding set of techniques, such as combinations of different methods with strong ability to provide more

quantitative and high-resolution images or new diagnostic information related to the biomechanical properties of tissues.

References

1. Samani A, Zubovits J, Plewes D. Elastic moduli of normal and pathological human breast tissues: an inversion-technique-based investigation of 169 samples. Phys Med Biol. 2007;52(6):1565–76.
2. Krouskop TA, Wheeler TM, Kallel F, et al. The elastic moduli of breast and prostate tissues under compression. Ultrason Imaging. 1998;20(4):260–74.
3. Wellman PS, Howe RD, Dalton E, et al. Breast tissue stiffness in compression is correlated to histological diagnosis. Harvard BioRobotics Laboratory, Technical Report, 1999.
4. Duck FA. Physical properties of tissues. New York: Academic; 1990.
5. Sarvazyan A, Hill CR. Physical chemistry of the ultrasound-tissue interaction. In: Hill CR, Bamber JC, Terhaar GR, editors. Physical principles of medical ultrasonics. 2nd ed. Chichester: Wiley; 2004. p. 223–35.
6. Parker KJ, Taylor LS, Gracewski S, et al. A unified view of imaging the elastic properties of tissue. J Acoust Soc Am. 2005;117(5):2705–12.
7. Greenleaf JF, Fatemi M, Insana M. Selected methods for imaging elastic properties of biological tissues. Annu Rev Biomed Eng. 2003;5:57–78.
8. Deffieux T, Montaldo G, Tanter M, et al. Shear wave spectroscopy for in vivo quantification of human soft tissues visco-elasticity. IEEE Trans Med Imaging. 2009;28(3):313–22.
9. Ophir J, Cespedes I, Ponnekanti H, et al. Elastography: a quantitative method for imaging the elasticity of biological tissues. Ultrason Imaging. 1991;13:111–34.
10. Parker KJ, Doyley MM, Rubens DJ. Imaging the elastic properties of tissue: the 20 year perspective. Phys Med Biol. 2011;56:R1–29.
11. Bamber JC, Bush NL. Freehand elasticity imaging using speckle decorrelation rate. Acoust Imaging. 1996;22:285–92.
12. Bamber JC, Barbone PE, Bush NL, et al. Progress in freehand elastography of the breast. IEICE Trans Inf Syst. 2002;E85D:5–14.
13. Shiina T, Doyley MM, Bamber JC. Strain imaging using combined RF and envelope autocorrelation processing. In: Proceedings of the 1996 IEEE Int Ultrasonics Symposium; 1996. p. 1331–6.
14. Varghese T, Ophir J. A theoretical framework for performance characterization of elastography: the strainfilter. IEEE Trans Ultrason Ferroelectr Freq Control. 1997;44:164–72.
15. Hall TJ, Zhu YN, Spalding CS. In vivo real-time freehand palpation imaging. Ultrasound Med Biol. 2003;29:427–35.
16. Shiina T, Nitta N, Ueno E, et al. Real time elasticity imaging using the combined autocorrelation method. J Med Ultrasonics. 2002;29:119–28.
17. Itoh A, Ueno E, Tohno E, et al. Breast disease: clinical application of US elastography for diagnosis. Radiology. 2006;239(2):341–50.
18. Ueno E, Tohno E, Bando H, et al. New quantitative method in breast elastography: fat lesion ration (FLR). Abstract of RSNA 2007; LL-BR2123-H04.
19. Farrokh A, Wojcinski S, Degenhardt F, et al. Diagnostic value of strain ratio measurement in the differentiation of malignant and benign breast lesion. Ultrashall Med. 2011;32(4):400–5.

20. Matsumura T. Measurement of elastic property of breast tissue for elasticity imaging. In: Proceedings of the 2009 IEEE Ultrasonics Symposium; 2009. p. 1451–4.

21. Thomas A, Warm M, Hoopmann M, et al. Tissue Doppler and strain imaging for evaluating tissue elasticity of breast lesions. Acad Radiol. 2007;14(5):522–9.

22. Nightingale K, Bentley R, Gregg ET. Observations of tissue response to acoustic radiation force: opportunities for imaging. Ultrason Imaging. 2002;24(3):129–38.

23. Nightingale K, Soo MS, Nightingale R, et al. Acoustic radiation force impulse imaging: in vivo demonstration of clinical feasibility. Ultrasound Med Biol. 2002;28(2):227–35.

24. Nyborg WLM, Litovitz T, Davis C. Acoustic streaming. In: Mason WP, editor. Physical acoustics. New York: Academic; 1965. p. IIA 265–331.

25. Torr GR. The acoustic radiation force. Am J Phys. 1984;52:402–8.

26. Cho Seung Hyun, Lee Jae Young, Han Joon Koo, et al. Acoustic radiation force impulse elastography for the evaluation of focal solid hepatic lesions: preliminary findings. Ultrasound Med Biol. 2010;36(2):202–8.

27. D'Onofrio M, Gallotti A, Salvia R, et al. Acoustic radiation force impulse (ARFI) ultrasound imaging of pancreatic cystic lesions. Eur J Radiol. 2011;80(2):241–4.

28. Gallotti A, D'Onofrio M, Mucelli RP. Acoustic radiation force impulse (ARFI) technique in the ultrasound study with virtual touch tissue quantification of the superior abdomen. Radiol Med. 2010;115(6):889–97.

29. Clevert DA, Stock K, Klein B. Evaluation of acoustic radiation force impulse (ARFI) imaging and contrast-enhanced ultrasound in renal tumors of unknown etiology in comparison to histological findings. Clin Hemorheol Microcirc. 2009;43(1–2):95–107.

30. Barr RG, Zhang Z. Effects of precompression on elasticity imaging of the breast-development of a clinically useful semi-quantitative method of precompression assessment. J Ultrasound Med. 2012;31:895–902.

31. Barnett SB, Duck F, Ziskin M. Recommendations on the safe use of ultrasound contrast agents. Ultrasound Med Biol. 2007;33:173–4.

32. Ultrasound Equipment and Safety Committee of The Japan Society of Ultrasonics in Medicine. Safe use of imaging equipment using acoustical radiation force. (http://www.jsum.or.jp/committee/m_and_s/acoustic_radiation.html).

33. Parker KJ, Huang SR, Musulin RA. Tissue response to mechanical vibrations for sonoelasticity imaging. Ultrasound Med Biol. 1990;16:241–6.

34. Sandrin L, Tanter M, Gennisson JL, et al. Shear elasticity probe for soft tissues with 1-D transient elastography. IEEE Trans UFFC. 2002;49(4):436–46.

35. Deffieux T, Montaldo G, Tanter M, et al. Shear wave spectroscopy for in vivo quantification of human soft tissues visco-elasticity. IEEE Trans Med Imaging. 2009;28(3):313–22.

36. Fujimoto K, Kato M, Kudo M, et al. Novel image analysis method using ultrasound elastography for noninvasive evaluation of hepatic fibrosis in patients with chronic hepatitis C. Oncology. 2013;84(suppl1):3–12.